miR-146a–Traf6 regulatory axis controls autoimmunity and myelopoiesis, but is dispensable for hematopoietic stem cell homeostasis and tumor suppression

Nathaniel Magilnick[a], Estefany Y. Reyes[a], Wei-Le Wang[a], Steven L. Vonderfecht[b], Jin Gohda[c], Jun-ichiro Inoue[d], and Mark P. Boldin[a,1]

[a]Department of Molecular and Cellular Biology, Beckman Research Institute, City of Hope, Duarte, CA 91010; [b]Division of Comparative Medicine, Beckman Research Institute, City of Hope, Duarte, CA 91010; [c]Research Center for Asian Infectious Diseases, Institute of Medical Science, University of Tokyo, Minato-ku, Tokyo 108-8639, Japan; and [d]Division of Cellular and Molecular Biology, Institute of Medical Science, University of Tokyo, Minato-ku, Tokyo 108-8639, Japan

Edited by Kenneth M. Murphy, Washington University in St. Louis, St. Louis, MO, and approved July 17, 2017 (received for review April 25, 2017)

***microRNA-146a* (*miR-146a*) has been previously implicated as an essential molecular brake, preventing immune overreaction and malignant transformation by attenuating NF-κB signaling, putatively via repression of the *Traf6* and *Irak1* genes. The exact contribution of *miR-146a*–mediated silencing of these genes to the control of immune activation is currently unknown. Therefore, we defined the role of the *miR-146a–Traf6* signaling axis in the regulation of immune homeostasis using a genetic epistasis analysis in *miR-146a*$^{-/-}$ mice. We have uncovered a surprising separation of functions at the level of miR-146a targets. Lowering the *Traf6* gene dose and consequent attenuation of NF-κB activation rescued several significant *miR-146a*$^{-/-}$ phenotypes, such as splenomegaly, aberrant myeloproliferation, and excessive inflammatory responses. In contrast, decreasing *Traf6* expression had no effect on the development of the progressive bone marrow failure phenotype, as well as lymphomagenesis in *miR-146a*$^{-/-}$ mice, indicating that miR-146a controls these biological processes through different molecular mechanisms.**

microRNA | inflammation | miR-146a | Traf6 | IFN-γ

Aberrant activation of immune cells is an underlying cause for numerous human pathologies, from systemic autoimmunity to cancer. *microRNA-146a* (*miR-146a*), a member of a large class of small-noncoding RNAs, has recently emerged as a critical immune regulator that helps prevent immune overreaction and malignant transformation (1). *miR-146a* is expressed primarily in cells of hematopoietic origin and is sharply up-regulated in response to microbial infection (2, 3). It functions as a negative feedback regulator of NF-κB signaling and, thus, mice that lack expression of this miRNA display exaggerated inflammatory responses to bacterial challenges and develop a systemic autoimmune disease over time (2, 4). Furthermore, dysregulation of *miR-146a* expression was implicated in the development of multiple autoimmune disorders in humans, including rheumatoid arthritis (5), systemic lupus erythematosus (6), and Sjogren's syndrome (7).

miR-146a plays an important role in the regulation of hematopoietic stem cell (HSC) homeostasis and myelopoiesis (8). Abrogation of *miR-146a* expression in mice results in splenomegaly due to massive myeloproliferation (2). Furthermore, *miR-146a* is recurrently down-regulated in the bone marrow (BM) of patients with myelodysplastic syndrome (MDS) (9, 10), while *miR-146a*–deficient mice (*miR-146a*$^{-/-}$) display an age-dependent, MDS-like HSC exhaustion and develop BM failure as they age (2).

Finally, *miR-146a* has a tumor-suppressor role and controls malignant transformation (2, 4, 11). Aged *miR-146a*$^{-/-}$ mice spontaneously develop tumors of myeloid and lymphoid origin. Moreover, accumulating evidence suggests that several types of human hematological and solid tumors display impaired miR-146a activity (12).

Thus, on balance, *miR-146a* is an essential regulator of immune cell activation, hematopoiesis, and cancer. Nevertheless, our understanding of the molecular mechanisms through which this miRNA elicits a wide range of biological activities remains poor. Studies performed in several laboratories have identified a gamut of miR-146a target genes in immune cells, including *Cxcr4*, *Irak1*, *Traf6*, *Card10*, *Fadd*, *Relb*, and *Stat1* (13–15). The two most validated miR-146a targets from this list are *Traf6* and *Irak1*, which encode adaptor proteins that function in a signaling hub that connects various immune receptors to the downstream signaling cascades, such as Jun amino-terminal kinase, p38 mitogen activated protein kinases (MAPK), extracellular signal-regulated kinase, and NF-κB activation pathways. The current molecular model suggests that *miR-146a* mediates its functions by attenuating *Traf6* and *Irak1* expression and subsequent dampening of NF-κB signal. However, this model has never been validated in vivo and, therefore, the physiological relevance of *Traf6* or *Irak1* gene silencing in the context of *miR-146a*–mediated regulation of immune functions is presently unknown.

To fill this knowledge gap, we performed a genetic epistasis analysis of the *miR-146a–Traf6* signaling axis in mice. Our findings suggest that tight control of *Traf6* expression is absolutely required for the *miR-146a*–mediated regulation of immune cell activation and myelopoiesis. Lowering the *Traf6* gene dose in *miR-146a*$^{-/-}$ mice rescued aberrant myeloproliferation and autoimmunity phenotypes. In contrast, we found that the

Significance

Aberrant inflammation is the root cause of numerous human diseases, from autoimmunity to cancer. *microRNA-146a* (*miR-146a*), a member of a large class of small regulatory RNAs, functions as a critical molecular brake on inflammation and malignant transformation. However, the molecular mechanism through which *miR-146a* exerts its regulatory activity in immune cells is unclear. Using mouse genetics, we have examined the role of the *miR-146a–Traf6* signaling axis and found that although this miRNA–target interaction is responsible for regulating normal myeloid cell development and autoimmunity, it is dispensable for hematopoietic stem cell homeostasis and tumor suppression.

Author contributions: N.M. and M.P.B. designed research; N.M., E.Y.R., and W.-L.W. performed research; J.G. and J.-i.I. contributed new reagents/analytic tools; N.M., S.L.V., and M.P.B. analyzed data; and N.M. and M.P.B. wrote the paper.

The authors declare no conflict of interest.

This article is a PNAS Direct Submission.

[1]To whom correspondence should be addressed. Email: mboldin@coh.org.

This article contains supporting information online at www.pnas.org/lookup/suppl/doi:10.1073/pnas.1706833114/-/DCSupplemental.

miR-146a–Traf6 regulatory axis is completely dispensable for the tumor-suppressive function of this miRNA and has little role in the maintenance of HSC homeostasis. Taken together, our results further elucidate the role that *miR-146a* plays in immune regulation and uncover the unexpected separation of function at the level of *miR-146a* targets that might explain the ability of this small regulatory RNA to control diverse immune functions.

Results

Deletion of One *Traf6* Allele in *miR-146a*–Deficient Mice Reduced TRAF6 Protein Expression to Near Wild-Type Levels. To define the role of *Traf6* in mediating physiological functions of *miR-146a*, we performed a genetic epistasis analysis of the *miR-146a–Traf6* signaling axis in mice. Because *miR-146a* deletion results in a modest *Traf6* derepression (2, 16), we reasoned that lowering the *Traf6* gene dose in *miR-146a*–deficient mice should reduce TRAF6 expression close to wild-type levels. To that end, we crossed *miR-146a*$^{-/-}$ (2) with mice carrying a targeted *Traf6* deletion allele (*Traf6*$^{+/-}$) (17). The genetic composition of the resulting *miR-146a*$^{-/-}$*Traf6*$^{+/-}$ compound mutant mice was validated by genomic PCR analysis (Fig. S1 *A* and *B*).

To examine how this genetic manipulation affected TRAF6 abundance, we compared the levels of TRAF6 protein in *miR-146a*$^{+/+}$, *miR-146a*$^{-/-}$, and *miR-146a*$^{-/-}$*Traf6*$^{+/-}$ splenocytes by Western blot analysis. In agreement with the previously published results (2, 16), we found a significant increase (~fivefold) in TRAF6 abundance in *miR-146a*$^{-/-}$ cells. In contrast, *miR-146a*$^{-/-}$*Traf6*$^{+/-}$ splenocytes expressed TRAF6 at near wild-type level (Fig. 1 *A* and *B*). Analysis of *Traf6* mRNA in *miR-146a*$^{+/+}$, *miR-146a*$^{-/-}$, and *miR-146a*$^{-/-}$*Traf6*$^{+/-}$ splenocytes revealed a similar pattern (Fig. 1*C*). Furthermore, we determined how lowering the *Traf6* gene dose impacts the activation of downstream signaling in *miR-146a*$^{-/-}$ cells. In agreement with previous reports (4, 16), we observed that abrogation of *miR-146a* activity results in the overactivation of the canonical

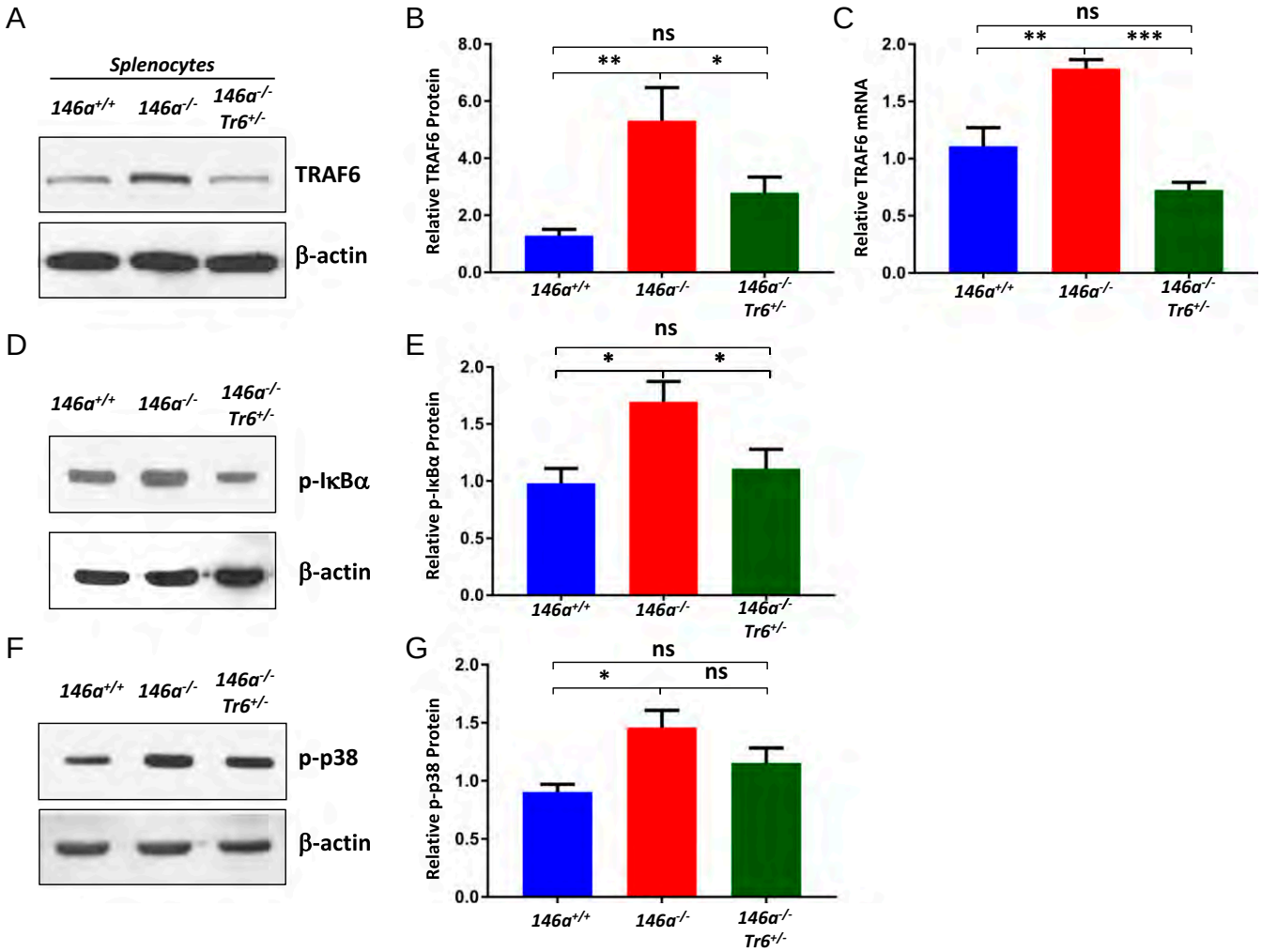

Fig. 1. Lowering the *Traf6* gene dose attenuates TRAF6 expression and the downstream NF-κB signaling in *miR-146a*$^{-/-}$ mice. (*A*) Western blot analysis of TRAF6 expression in *miR-146*$^{+/+}$, *miR-146a*$^{-/-}$, and *miR-146a*$^{-/-}$*Traf6*$^{+/-}$ splenocytes. (*B*) Quantification of TRAF6 protein expression in *miR-146*$^{+/+}$ ($n = 11$), *miR-146a*$^{-/-}$ ($n = 14$), and *miR-146a*$^{-/-}$*Traf6*$^{+/-}$ ($n = 14$) splenocytes. (*C*) Quantitative RT-PCR analysis of *Traf6* mRNA levels in *miR-146*$^{+/+}$, *miR-146a*$^{-/-}$, and *miR-146a*$^{-/-}$*Traf6*$^{+/-}$ splenocytes ($n = 5$ per group). (*D*) Western blot analysis of phosphorylated IκBα in *miR-146*$^{+/+}$, *miR-146a*$^{-/-}$, and *miR-146a*$^{-/-}$*Traf6*$^{+/-}$ splenocytes. (*E*) Quantification of phosphorylated IκBα in *miR-146*$^{+/+}$, *miR-146a*$^{-/-}$, and *miR-146a*$^{-/-}$*Traf6*$^{+/-}$ splenocytes ($n = 6$). (*F*) Western blot analysis of phosphorylated p38 MAPK in *miR-146*$^{+/+}$, *miR-146a*$^{-/-}$, and *miR-146a*$^{-/-}$*Traf6*$^{+/-}$ splenocytes. (*G*) Quantification of phosphorylated p38 MAPK in *miR-146*$^{+/+}$, *miR-146a*$^{-/-}$, and *miR-146a*$^{-/-}$*Traf6*$^{+/-}$ splenocytes ($n = 6$ per group). TRAF6, phospho-IκBα, and phospho-p38 values were obtained from scanned X-ray films using ImageJ software. Each sample was first normalized to β-actin that was used as loading control. Data are shown as mean ± SEM. *P* values were calculated using a standard one-way ANOVA test. *$P \le 0.05$; **$P \le 0.01$; ***$P \le 0.001$; ns, not significant.

NF-κB signaling cascade (Fig. 1 *D* and *E*). However, deletion of one *Traf6* allele significantly attenuated the aberrant NF-κB signal in *miR-146a*$^{-/-}$ cells (Fig. 1 *D* and *E* and Fig. S1*C*). Western blot analysis of p38 MAPK activation in *miR-146a*$^{-/-}$ *Traf6*$^{+/-}$ splenocytes, another key signaling pathway that is triggered by TRAF6 (18), detected a trend for lower activity in comparison with *miR-146a*$^{-/-}$ cells (Fig. 1 *F* and *G*). Thus, collectively, our results strongly indicate that *Traf6* haploinsufficiency may effectively restore the normal function of the *miR-146a–Traf6* regulatory axis in the context of the *miR-146a*–null phenotype.

Lowering the *Traf6* Gene Dose Rescued Aberrant Myeloproliferation in *miR-146a*$^{-/-}$ Mice. One of the most profound phenotypic changes in *miR-146a*$^{-/-}$ mice is a myeloproliferative disorder that is grossly manifested by a progressive splenomegaly. To investigate how lowering the *Traf6* gene dose impacts aberrant myeloproliferation in *miR-146a*$^{-/-}$ mice, we performed a morphological analysis of aged (8- to 10-mo-old) cohorts of female *miR-146a*$^{+/+}$, *miR-146a*$^{-/-}$, and *miR-146a*$^{-/-}$*Traf6*$^{+/-}$ mice. As expected, we observed a significant splenomegaly (~fourfold increase in spleen weight) in *miR-146a*$^{-/-}$ animals (Fig. 2 *A* and *B*), while *miR-146a*$^{-/-}$*Traf6*$^{+/-}$ mice displayed a partial rescue of this defect (~twofold spleen weight increase in comparison with the *miR-146a*$^{+/+}$ group) (Fig. 2 *A* and *B*). Furthermore, we also found a marked decrease in the total number of cells in *miR-146a*$^{-/-}$*Traf6*$^{+/-}$ spleen in comparison with *miR-146a*$^{+/+}$ organs (Fig. 2*C*). Of note, the spleen weight and cellularity in the *miR-146a*$^{+/+}$*Traf6*$^{+/-}$ cohort were indistinguishable from *miR-146a*$^{+/+}$ animals (Fig. 2 *A–C*).

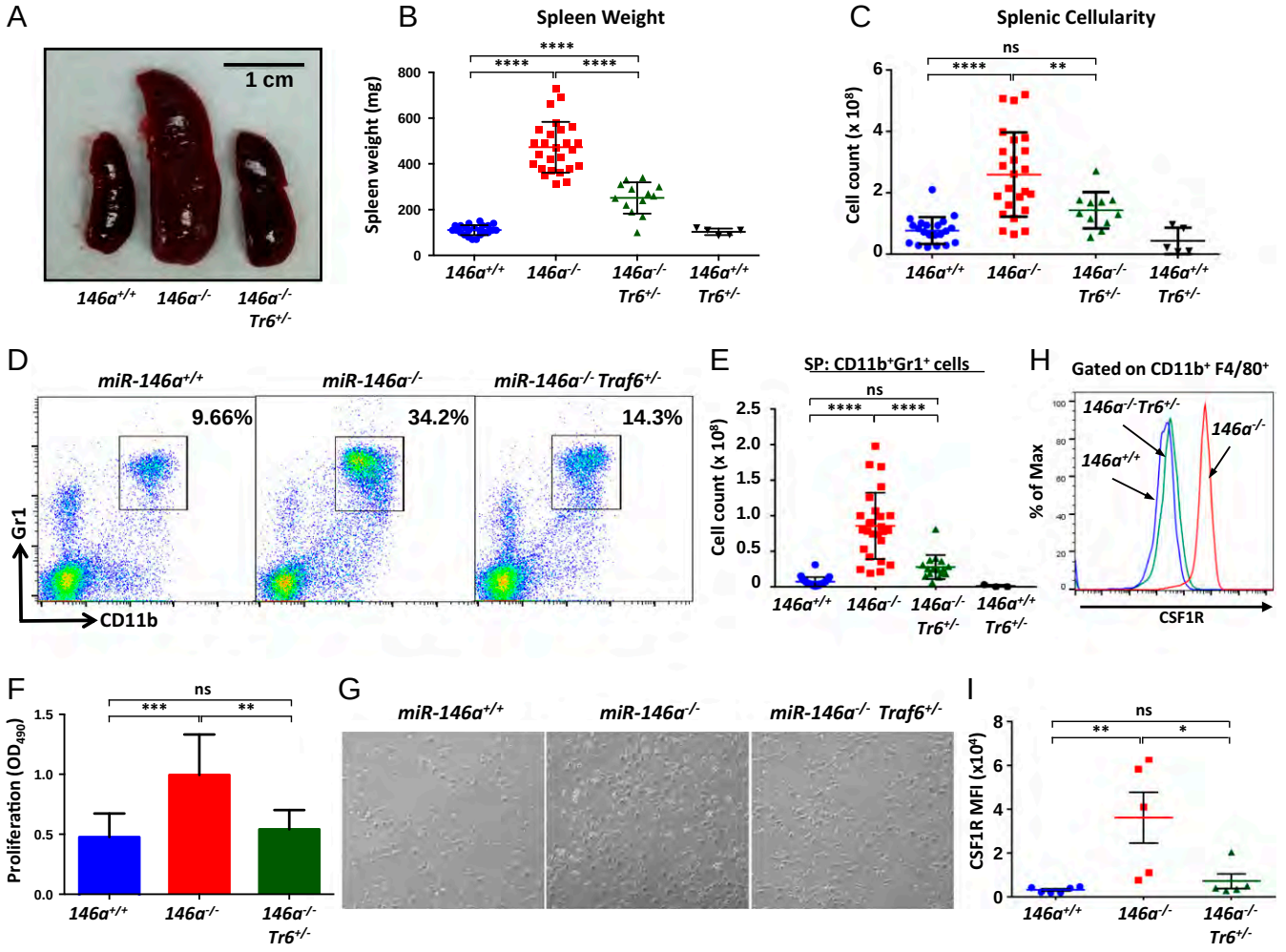

Fig. 2. *miR-146a*–dependent attenuation of *Traf6* is required for control of myeloproliferation. (*A–C*) Rescue of the splenomegaly defect in *miR-146a*$^{-/-}$*Traf6*$^{+/-}$ mice. (*A*) Photograph of spleens from *miR-146*$^{+/+}$, *miR-146a*$^{-/-}$, and *miR-146a*$^{-/-}$*Traf6*$^{+/-}$ mice. Spleen weight (*B*) and cellularity (*C*) in 9- to 10-mo-old female *miR-146*$^{+/+}$, *miR-146a*$^{-/-}$, and *miR-146a*$^{-/-}$*Traf6*$^{+/-}$ mice ($n \geq 5$ per group). (*D* and *E*) Rescue of the myeloproliferation phenotype in *miR-146a*$^{-/-}$*Traf6*$^{+/-}$ mice. (*D*) Flow cytometry analysis of splenocytes from *miR-146*$^{+/+}$, *miR-146a*$^{-/-}$, and *miR-146a*$^{-/-}$*Traf6*$^{+/-}$ mice using antibodies against CD11b and Gr1. Immature myeloid cells (CD11b^{+}Gr1^{+}) are gated, and numbers indicate the percentage of cells in the gate. (*E*) Total number of CD11b^{+}Gr1^{+} cells in spleens of 9- to 10-mo-old female *miR-146*$^{+/+}$, *miR-146a*$^{-/-}$, *miR-146a*$^{-/-}$*Traf6*$^{+/-}$, and *miR-146*$^{+/+}$*Traf6*$^{+/-}$ mice ($n \geq 16$ per group). (*F* and *G*) Deletion of one *Traf6* allele attenuates proliferation capacity of *miR-146a*$^{-/-}$ macrophages. (*F*) Quantification of BMDM proliferation. Macrophages were derived from *miR-146*$^{+/+}$, *miR-146a*$^{-/-}$, and *miR-146a*$^{-/-}$*Traf6*$^{+/-}$ BM in the presence of 50 ng/mL M-CSF for 3 d before their proliferation ability was measured using the MTS assay. Data were combined from three independent experiments ($n \geq 7$ per group). (*G*) Representative pictures of *miR-146*$^{+/+}$, *miR-146a*$^{-/-}$, and *miR-146a*$^{-/-}$*Traf6*$^{+/-}$ BMDM cultures. (Magnification: 40×.) (*H*) Flow cytometry analysis of CSF1R expression on *miR-146*$^{+/+}$ (blue line), *miR-146a*$^{-/-}$ (red line), and *miR-146a*$^{-/-}$*Traf6*$^{+/-}$ (green line) macrophages. BMDMs were derived as described in *F*. Cells were pregated for the expression of CD11b and F4/80 markers first. (*I*) Quantification of cell surface CSF1R expression on *miR-146*$^{+/+}$, *miR-146a*$^{-/-}$, and *miR-146a*$^{-/-}$*Traf6*$^{+/-}$ BMDMs ($n \geq 5$ per group). MFI, mean fluorescent intensity. Data are shown as mean ± SD. *P* values were calculated using a standard one-way ANOVA test. *$P \leq 0.05$; **$P \leq 0.01$; ***$P \leq 0.001$; ****$P \leq 0.0001$; ns, not significant; SP, spleen.

Using flow cytometry, we quantified the accumulation of immature myeloid cells in the spleens of aged mice and determined that lowering the *Traf6* gene dose reduces the frequency and absolute number of $CD11b^{+}Gr1^{+}$ myeloid cells to near wild-type levels, suggesting a clear rescue of this *miR-146a*$^{-/-}$ phenotype (Fig. 2 *D* and *E*).

To further characterize the role of the *miR-146a–Traf6* signaling axis in the regulation of myeloid development, we generated BM-derived macrophages (BMDMs) from the three strains of mice and assessed their proliferative potential in vitro. Consistent with our previous findings (2), *miR-146a*$^{-/-}$ BMDMs displayed a clear proliferative advantage over wild-type BMDMs after 3 d in culture (Fig. 2 *F* and *G*). On the other hand, *miR-146a*$^{-/-}$*Traf6*$^{+/-}$ macrophages divided much slower and resembled wild-type cells in their proliferation capacity (Fig. 2 *F* and *G*). We have previously linked enhanced proliferation of *miR-146a*$^{-/-}$ BMDMs to an increase in colony stimulating factor receptor 1 (CSF1R) expression (2). In agreement with this notion, we found that the cell surface levels of CSF1R on *miR-146a*$^{-/-}$*Traf6*$^{+/-}$ macrophages were significantly down-regulated in comparison with *miR-146a*$^{-/-}$ cells (Fig. 2 *H* and *I*).

***miR-146a*–Mediated Control of *Traf6* Expression Is Required for the Attenuation of Proinflammatory Cytokine Responses, Control of T Cell Tolerance, and Prevention of Autoimmunity.** Previous studies have firmly established *miR-146a* as a negative regulator of inflammation and autoimmunity (2, 13, 16). Because of its critical role in the activation of NF-κB signaling, *Traf6* has long been proposed as a key molecular target through which *miR-146a* controls immune responses. However, formal in vivo evidence supporting this notion is missing. To determine the role of the *miR-146a–Traf6* axis in the regulation of immune responses, we characterized several aspects of innate and adaptive immunity in *miR-146a*$^{-/-}$*Traf6*$^{+/-}$ mice.

First, we examined how the compound mutant mice respond to a systemic bacterial endotoxin challenge. Age- and gender-matched

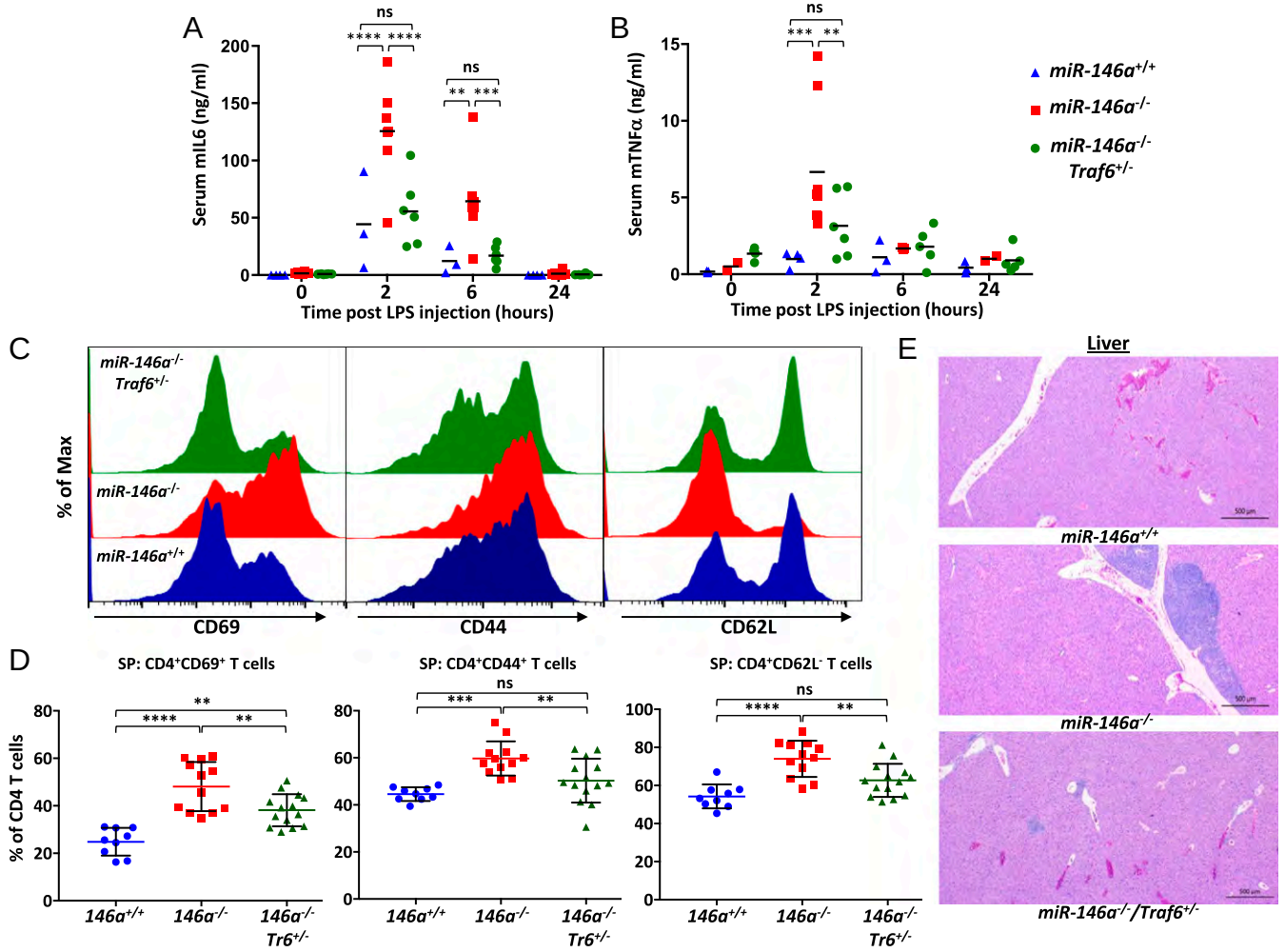

Fig. 3. Lowering the *Traf6* gene dose rescues aberrant inflammation phenotype in *miR-146a*–null mice. (*A* and *B*) Normal cytokine response to bacterial endotoxin challenge in *miR-146a*$^{-/-}$*Traf6*$^{+/-}$ mice. Serum levels of IL-6 (*A*) and TNF-α (*B*) cytokines in *miR-146*$^{+/+}$ ($n \geq 3$), *miR-146a*$^{-/-}$ ($n = 6$), and *miR-146a*$^{-/-}$*Traf6*$^{+/-}$ ($n = 6$) mice challenged intraperitoneally with a sublethal LPS (1 mg/kg) dose. Peripheral blood was collected at the indicated time points and cytokine concentrations were analyzed in the serum by sandwich ELISA. All mice were female and aged 3–4 mo. (*C* and *D*) *Traf6* haploinsufficiency reverts the hyperactivated state of peripheral *miR-146a*$^{-/-}$ T cells. (*C*) FACS analysis of CD69, CD44, and CD62L activation markers on $CD4^{+}$ T cells isolated from *miR-146*$^{+/+}$ (blue plots), *miR-146a*$^{-/-}$ (red plots), and *miR-146a*$^{-/-}$*Traf6*$^{+/-}$ (green plots) spleens. (*D*) Quantification of CD69, CD44, and CD62L expression levels on $CD4^{+}$ T cells isolated from *miR-146*$^{+/+}$, *miR-146a*$^{-/-}$, and *miR-146a*$^{-/-}$*Traf6*$^{+/-}$ spleens ($n > 9$ animals for all genotypes, female mice aged 9–10 mo). Values are reported as percent of $CD4^{+}$ T cells. (*E*) Lowering the *Traf6* gene dose in *miR-146a*$^{-/-}$ mice decreases lymphohistiocytic infiltrates in liver. Representative H&E-stained sections from 9- to 10-mo-old *miR-146*$^{+/+}$, *miR-146a*$^{-/-}$, *miR-146a*$^{-/-}$*Traf6*$^{+/-}$ mice. Data are shown as mean ± SD. *P* values were calculated using either standard one-way or two-way ANOVA tests. $^{**}P \leq 0.01$; $^{***}P \leq 0.001$; $^{****}P \leq 0.0001$; ns, not significant; SP, spleen. (Magnification: 20×.)

cohorts of *miR-146a*$^{+/+}$, *miR-146a*$^{-/-}$, and *miR-146a*$^{-/-}$*Traf6*$^{+/-}$ mice were challenged with a sublethal dose of bacterial lipopolysaccharides (LPS) and levels of proinflammatory cytokines in the serum were measured by ELISA. In agreement with previously published results (2), *miR-146a*$^{-/-}$ mice mounted an exaggerated proinflammatory cytokine response following LPS injection, manifested by a significantly elevated production of IL-6 and TNF-α proteins in comparison with wild-type animals (Fig. 3 *A* and *B*). On the other hand, *miR-146a*$^{-/-}$*Traf6*$^{+/-}$ mice displayed a marked reduction in the production of these cytokines to near wild-type levels (Fig. 3 *A* and *B*), suggesting that *miR-146a* indeed controls Toll-like receptor (TLR)-mediated inflammatory responses by attenuating TRAF6 protein levels.

Abrogation of *miR-146a* expression was reported to result in the loss of peripheral T cell tolerance and subsequent development of the autoimmune disease (2). Analysis of the peripheral T cells in *miR-146a*$^{-/-}$ mice by flow cytometry revealed that the majority of splenic CD4^{+} T cells displayed an activated effector status as characterized by the loss of L-Selectin (CD62L), and a gain of PGP-1 (CD44) and CD69 expression (Fig. 3 *C* and *D*). In contrast, examination of the T cell populations in *miR-146a*$^{-/-}$*Traf6*$^{+/-}$ mice found that lowering the *Traf6* gene dose rescues this defect and leads to a significant reduction in the amount of the activated effector T cells (Fig. 3 *C* and *D*). Furthermore, histological analysis of liver sections from *miR-146a*$^{-/-}$*Traf6*$^{+/-}$ mice revealed reduced lymphohistiocytic infiltrates compared with *miR-146a*$^{-/-}$ mice (Fig. 3*E*). Collectively, our results suggest that the *miR-146a–Traf6* signaling axis plays a crucial role in maintaining the homeostasis of the immune system and preventing development of autoimmunity.

The *miR-146a–Traf6* Regulatory Axis Is Dispensable for Tumor Suppression. *miR-146a* was previously implicated in the regulation of tumorigenesis (2, 4); however, our molecular understanding of its tumor-suppressor activity is incomplete. Since chronic inflammation often promotes malignant transformation and because our findings suggest that the *miR-146a–Traf6* signaling axis is essential for the regulation of inflammatory responses, we investigated the role of *Traf6* in mediating the tumor-suppressor activity of *miR-146a*. Aged *miR-146a*$^{-/-}$ mice develop spontaneous tumors of both lymphoid and myeloid origin, however with relatively low penetrance and long latency (2, 4). Thus, to make our analysis of tumorigenesis in *miR-146a*$^{-/-}$ mice more robust, we chose to take advantage of the Eμ-myc transgenic mouse model. Eμ-myc transgenic mice carry a *c-myc* oncogene driven by the Ig heavy-chain enhancer and invariably develop a mix of pre-B and mature B cell lymphomas with a latency of about 24 wk (19). The protracted latent period before the onset of frank disease in this model likely reflects the inability of *c-myc* overexpression to initiate malignant transformation on its own, requiring cooperation from additional genetic lesions (20). Many aspects of the lymphomas that Eμ-myc mice develop resemble known features of human disease, including progression through a distinct premalignant phase (21).

We bred Eμ-myc transgenic mice onto both the *miR-146a*$^{-/-}$ and *miR-146a*$^{-/-}$*Traf6*$^{+/-}$ backgrounds and generated Tg(Eμ-myc);*miR-146a*$^{-/-}$ and Tg(Eμ-myc);*miR-146a*$^{-/-}$*Traf6*$^{+/-}$ compound mutant mice. To determine whether *miR-146a* abrogation affects disease onset and mortality, we aged large cohorts of the compound mutant mice and monitored them for the appearance of lymph node tumors as well as signs of systemic illness. We found that Tg(Eμ-myc);*miR-146a*$^{-/-}$ mice displayed a significant increase in mortality in comparison with control Eμ-myc transgenic animals (the median time of survival dropped from 24 wk down to 15 wk) (Fig. 4*A*). Moreover, immunophenotyping of *miR-146a*–deficient and *miR-146a*–proficient lymphomas revealed a change in the maturation status of malignant B cells: Tg(Eμ-myc);*miR-146a*$^{-/-}$ tumors were derived predominantly from immature B cells (B220^{+}IgM^{+}), while the majority of tumors

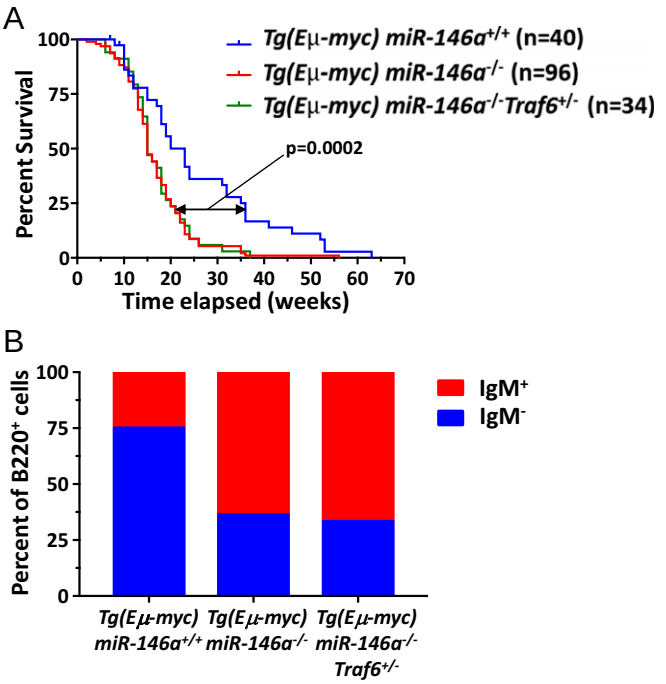

Fig. 4. *miR-146a* does not require *Traf6* to exert its tumor-suppressive function. (*A*) Survival of female Tg(Eμ-Myc);*miR-146a*$^{+/+}$ (n = 40), Tg(Eμ-Myc);*miR-146a*$^{-/-}$ (n = 96), and Tg(Eμ-Myc);*miR-146a*$^{-/-}$*Traf6*$^{+/-}$ (n = 34) mice. Animals were monitored daily and euthanized once the tumor became palpable or the animals appeared to be in distress as per standard IACUC guidelines for care of tumor-bearing mice. The survival curve comparison was calculated using a Mantel–Cox (log rank) test, P = 0.0002. (*B*) FACS analysis of tumors from female Tg(Eμ-Myc);*miR-146a*$^{+/+}$ (n = 9), Tg(Eμ-Myc);*miR-146a*$^{-/-}$ (n = 14), and Tg(Eμ-Myc);*miR-146a*$^{-/-}$*Traf6*$^{+/-}$ (n = 11) mice using anti-B220 and anti-IgM antibodies. Cells were pregated for the expression of CD19 first. The IgM marker defines B cell development stage: early B cell precursors were identified as CD19^{+}B220^{+}IgM^{-}, and immature B cells were identified as CD19^{+}B220^{+}IgM^{+}.

in Tg(Eμ-myc) mice originated from the early B cell precursors (B220^{+}IgM^{-}) (Fig. 4*B*). These observations are in good agreement with the recent findings by Contreras et al. (11), indicating that *miR-146a* loss accelerates MYC-driven lymphoma development.

Interestingly, lowering the *Traf6* gene dose in Tg(Eμ-myc);*miR-146a*$^{-/-}$ mice did not rescue this phenotype, because Tg(Eμ-myc);*miR-146a*$^{-/-}$*Traf6*$^{+/-}$ and Tg(Eμ-myc);*miR-146a*$^{-/-}$ mice were found to display identical mortality rates, as well as similar makeup of B cell lymphomas (Fig. 4). Together, our findings suggest that *miR-146a*–mediated control of *Traf6* expression and downstream inflammatory responses is dispensable for the tumor-suppressor activity of this miRNA, indicating that miR-146a must engage other, perhaps not yet identified, molecular targets to exert its regulatory effect on malignant transformation.

Lowering the *Traf6* Gene Dose Does Not Prevent HSC Depletion and Development of BM Failure in *miR-146a*$^{-/-}$ Mice. One of the more profound defects found in mice lacking a functional *miR-146a* gene is the progressive impairment of hematopoiesis. By 8 mo of age, *miR-146a*$^{-/-}$ mice display severe anemia, leukopenia, and thrombocytopenia (Fig. 5 *A–D*) that are consistent with the BM failure typically found in MDS or aplastic anemia (AA) (2, 10). This progressive pancytopenia is a consequence of the destruction of the normal HSC niche (10). Using the Signaling Lymphocyte Activation Molecule (SLAM) system of defining undifferentiated stem and progenitor cells, we confirmed the findings by Zhao et al. (10) that aged *miR-146a*$^{-/-}$ mice have a drastically reduced population of long-term HSCs (LT-HSCs) in

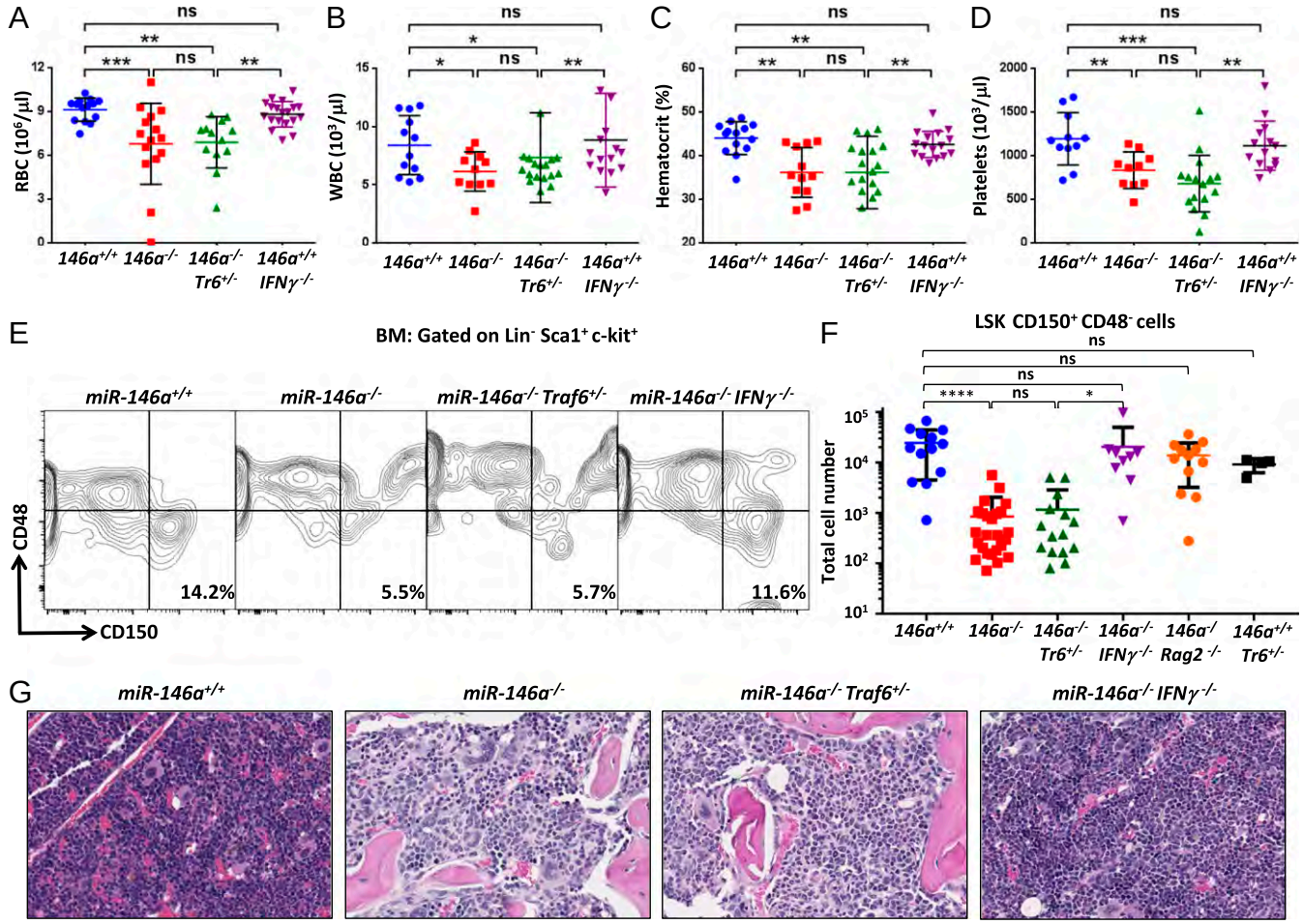

Fig. 5. BM failure in *miR-146a*$^{-/-}$ mice is rescued by *IFN-γ* ablation, but not by lowering the *Traf6* gene dose. (*A–D*) Complete blood count tests of terminal blood collected from 9- to 10-mo-old female *miR-146*$^{+/+}$, *miR-146a*$^{-/-}$, *miR-146a*$^{-/-}$*Traf6*$^{+/-}$, and *miR-146a*$^{-/-}$*IFN-γ*$^{-/-}$ mice ($n \geq 10$ for each group). (*A*) Absolute red blood counts. (*B*) Absolute white blood counts (WBC). (*C*) Blood hematocrit. (*D*) Absolute platelet counts. (*E* and *F*) Analysis of LT-HSC cells from the BM of 9- to 10-mo-old female *miR-146*$^{+/+}$, *miR-146a*$^{-/-}$, *miR-146a*$^{-/-}$*Traf6*$^{+/-}$, and *miR-146a*$^{-/-}$*IFNγ*$^{-/-}$ mice. Lineage depleted cells (Lin$^-$) from BM were analyzed by FACS using anti–c-kit, -Sca1, -CD150, -CD48 antibodies. (*E*) Representative FACS analysis using the SLAM markers to identify the LT-HSC population as Lin$^-$c-kit$^+$Sca1$^+$CD150$^+$CD48$^-$. Numbers indicate frequency of LT-HSCs. (*F*) Quantification of LT-HSCs using the SLAM marker system in 9- to 10-mo-old *miR-146*$^{+/+}$, *miR-146a*$^{-/-}$, *miR-146a*$^{-/-}$*Traf6*$^{+/-}$, *miR-146a*$^{-/-}$*IFNγ*$^{-/-}$, *miR-146a*$^{-/-}$*Rag2*$^{-/-}$, and *miR-146a*$^{+/+}$*Traf6*$^{+/-}$ BM ($n \geq 13$ for all groups except *miR-146a*$^{+/+}$*Traf6*$^{+/-}$ $n = 4$). (*G*) Representative H&E-stained sections of tibias from 9- to 10-mo-old female *miR-146*$^{+/+}$, *miR-146a*$^{-/-}$, *miR-146a*$^{-/-}$*Traf6*$^{+/-}$, and *miR-146a*$^{-/-}$*IFN-γ*$^{-/-}$ mice. Note that BM in *miR-146a*$^{-/-}$ and *miR-146a*$^{-/-}$*Traf6*$^{+/-}$ mice is markedly hypocellular, whereas *miR-146a*$^{-/-}$*IFN-γ*$^{-/-}$ BM appears closer to normal and is only minimally hypocellular. Data are shown as mean ± SD. *P* values were calculated using standard one-way ANOVA tests. *$P \leq 0.05$; **$P \leq 0.01$; ***$P \leq 0.001$; ****$P \leq 0.0001$; ns, not significant. (Magnification: 40×.)

the BM (Fig. 5 *E* and *F*). Furthermore, we also observed that BM architecture in aged *miR-146a*–deficient mice undergoes significant remodeling characterized by marked hypocellularity and morphologic features consistent with myelofibrosis (Fig. 5*G*). Surprisingly, in contrast to the above-described analyses of the myeloproliferation and autoimmunity defects, we found that *Traf6* haploinsufficiency in *miR-146a*$^{-/-}$ mice had no impact on the development of the BM failure phenotype. Aged *miR-146a*$^{-/-}$*Traf6*$^{+/-}$ mice have significantly diminished numbers of LT-HSCs in the BM (Fig. 5 *E* and *F*) and, consequently, display no rescue of the pancytopenia that is characteristic for *miR-146a*–deficient mice (Fig. 5 *A–D*). Thus, our findings argue that *miR-146a* most likely uses a *Traf6*-independent molecular mechanism for the regulation of HSC homeostasis.

Excessive IFN-γ Production by BM-Resident T Cells Destroys HSC Niche in *miR-146a*$^{-/-}$ Mice. IFN-γ has a well-documented role in suppressing HSC maintenance and self-renewal (22, 23). Moreover, AA patients (who develop BM failure because of HSC exhaustion) frequently display elevated levels of IFN-γ in the peripheral blood, as well as impaired colony-forming potential of BM cells, which can be restored by treatment with IFN-γ neutralizing antibodies (24). Interestingly, *miR-146a*–deficient T cells are known to produce aberrantly high levels of IFN-γ that were shown to contribute to the loss of immunological tolerance (13, 16). These findings prompted us to hypothesize that dysregulation of IFN-γ production mediates HSC destruction in *miR-146a*$^{-/-}$ mice. To probe this notion genetically, we cross-bred *IFN-γ*$^{-/-}$ mice (25) with *miR-146a*$^{-/-}$ mice and generated *miR-146a*$^{-/-}$*IFN-γ*$^{-/-}$ double-knockout mice. Our analysis of aged *miR-146a*$^{-/-}$*IFN-γ*$^{-/-}$ mice revealed normal peripheral blood cell counts (Fig. 5 *A–D*), suggesting that *IFN-γ* ablation can rescue the BM failure defect caused by *miR-146a* deficiency. In agreement with this conclusion, we also found that the number of LT-HSCs in *miR-146a*$^{-/-}$*IFN-γ*$^{-/-}$ BM rebounded to near wild-type level (Fig. 5 *E* and *F*), while histological analysis of the double-knockout BM revealed partial rescue of the hypocellulartity and apparent fibrosis (Fig. 5*G*). Depletion of B and T lymphocytes

via *Rag2* deletion also prevented LT-HSC destruction in *miR-146a*$^{-/-}$ BM (Fig. 5*F*), pointing to an HSC-extrinsic nature of this defect.

Since activated T cells are considered the main source of IFN-γ in the body, we examined production of this proinflammatory cytokine by BM-resident *miR-146a*$^{-/-}$ T cells. Of note, CD3^{+} T cells were previously reported to constitute 1–5% of all mononuclear cells in the mouse BM (26). Using a flow cytometry protocol for intracellular staining, we detected slightly elevated basal level of IFN-γ production in CD8^{+} T cells isolated from *miR-146a*$^{-/-}$ BM (Fig. S2 *A* and *B*). IFN-γ expression in BM-resident *miR-146a*$^{-/-}$ CD4^{+} T cells followed the same trend, but the difference was not statistically significant (Fig. S2 *C* and *D*). However, stimulation with phorbol 12-myristate 13-acetate and ionomycin confirmed that both CD8^{+} and CD4^{+} T cells from *miR-146a*$^{-/-}$ BM have a much greater IFN-γ productive potential than wild-type cells (Fig. 6). Interestingly, we found that IFN-γ overproduction by BM-resident *miR-146a*$^{-/-}$ T cells was largely refractory to the lowering of the *Traf6* gene dose (Fig. 6 and Fig. S2 *A*–*D*). The exaggerated production of IFN-γ in response to stimulation was also observed in *miR-146*–deficient T cells isolated from the spleen, although the defect was slightly less pronounced than in BM-resident T cells (Fig. S3). Natural killer (NK) cells are another known source of IFN-γ in the body; however, our analysis revealed that IFN-γ secretion by NK cells from *miR-146a*$^{-/-}$ BM is comparable to wild-type cells (Fig. S2*E*). Thus, our experiments suggest that *Traf6*-independent dysregulation of *IFN-γ* expression in BM-resident T cells is responsible for the destruction of the HSC niche in *miR-146a*$^{-/-}$ mice.

Discussion

Previous work by us and other investigators has established *miR-146a* as an essential immune regulator that controls activation and malignant transformation of immune cells (2, 13, 16). However, the exact molecular mechanism through which *miR-146a* exerts its numerous regulatory activities is unclear. In the present study using genetic epistasis analysis, we have examined the role of *Traf6*, one of the most validated miR-146a targets, in mediating some of the known physiological functions of this miRNA. Our findings uncovered an unexpected separation of function at the level of miR-146a target genes. On the one hand, lowering of the *Traf6* gene dose effectively rescued the myeloproliferative and autoimmune phenotypes in *miR-146a*–deficient mice. In contrast, the *Traf6* halploinsufficiency had little effect on the progressive HSC destruction and subsequent development of BM failure in *miR-146a*–null mice. Furthermore, we found that attenuation of *Traf6* expression by miR-146a is largely dispensable for the tumor-suppressive activity of this miRNA in B lymphocytes.

TRAF6 is a versatile adapter protein with a K63-linked ubiquitin ligase activity that triggers NF-κB and MAPK signaling downstream of a multitude of immune receptors (27). As evidenced by the overexpression studies, TRAF6 abundance has to be tightly regulated to prevent aberrant NF-κB signaling (28, 29). Hence, miR-146a, which binds to three evolutionary conserved 8-mer "seed" sequences in the *Traf6* 3′UTR (3), has evolved as a crucial molecular brake on *Traf6* expression and subsequent NF-κB activation. Because NF-κB signaling plays an essential role in the initiation and

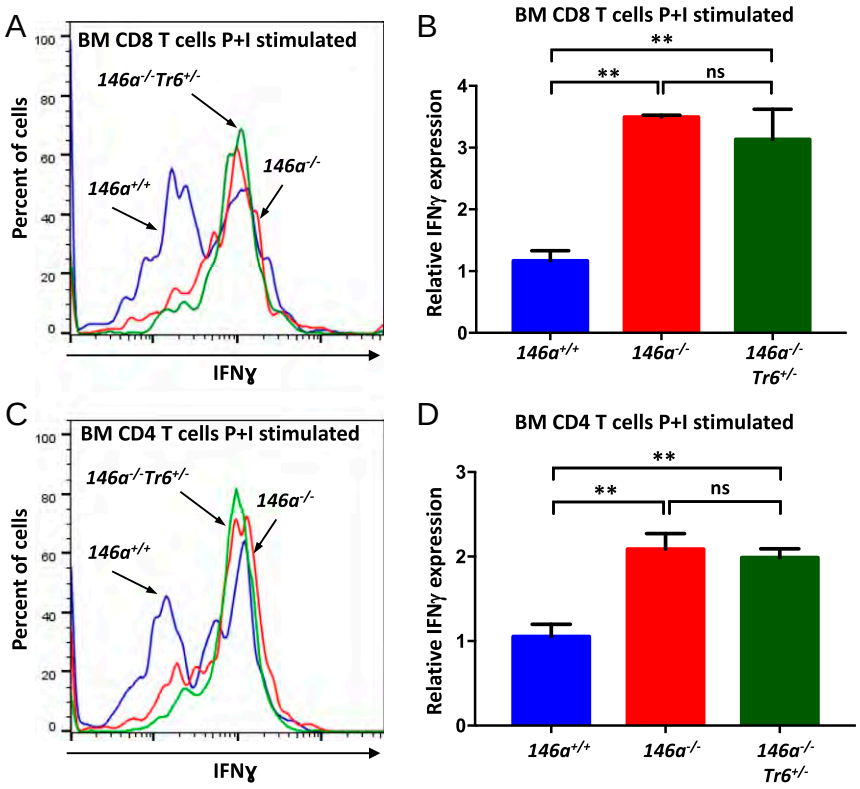

Fig. 6. BM-resident T cells are the main producers of aberrant IFN-γ driving the HSC destruction in *miR-146a*$^{-/-}$ mice. FACS analysis of IFN-γ production by CD8^{+} (*A* and *B*) and CD4^{+} (*C* and *D*) T cells isolated from *miR-146*$^{+/+}$, *miR-146a*$^{-/-}$, *miR-146a*$^{-/-}$*Traf6*$^{+/-}$ BM. BM cells harvested from 8-wk-old female mice were stimulated with phorbol 12-myristate 13-acetate and ionomycin (P+I) for 4 h and analyzed by flow cytometry for intracellular IFN-γ expression. Representative FACS plots showing IFN-γ expression in stimulated CD8^{+} (*A*) and CD4^{+} (*C*) T cells from *miR-146*$^{+/+}$ (blue line), *miR-146a*$^{-/-}$ (red line), and *miR-146a*$^{-/-}$*Traf6*$^{+/-}$ (green line) BM. Quantification of intracellular IFN-γ expression in stimulated CD8^{+} (*B*) and CD4^{+} (*D*) T cells from *miR-146*$^{+/+}$, *miR-146a*$^{-/-}$, and *miR-146a*$^{-/-}$*Traf6*$^{+/-}$ BM. IFN-γ MFI values were calculated using the FlowJo X software and then were normalized to *miR-146*$^{+/+}$ samples. Data are representative of at least three different experiments with $n \geq 3$ for each genotype. Data are shown as mean ± SD. *P* values were calculated using standard one-way ANOVA tests. $^{**}P \leq 0.01$; ns, not significant.

execution of immune responses, *Traf6* is often viewed as a key miR-146a target, through which miR-146a mediates most, if not all, of its immunomodulatory activities. However, our epistasis analysis in *miR-146a*–deficient mice challenges this notion and suggests that miR-146a engages additional molecular targets to mediate its biological functions.

Confirming the importance of the *miR-146a–Traf6* regulatory axis, our findings implicate *Traf6* derepression and subsequent NF-κB overactivation as the main drivers of aberrant myeloproliferation and autoimmunity in *miR-146a*$^{-/-}$ mice. This conclusion is in good agreement with the known role of the NF-κB signaling pathway in myeloid cell differentiation and proinflammatory signaling (30). For example, ablation of *IκBα*, a critical NF-κB pathway inhibitor, was previously shown to result in aberrant granulocytopoiesis because of constitutive NF-κB activation (30–32). Additionally, lowering of the *Nfkb1* gene dose in *miR-146a*–null mice was reported to partially rescue the splenomegaly and abnormal accumulation of CD11b^{+}Gr1^{+} myeloid cells (10).

Constitutive NF-κB activation is a hallmark of many hematopoietic and solid tumors (33–37). Therefore, the significant susceptibility of aged *miR-146a*–deficient mice to cancer was often considered in the context of the TRAF6–NF-κB signaling axis dysregulation. However, our genetic dissection of the tumor-suppressor activity of *miR-146a* in B cells does not support this hypothesis. Lowering of the *Traf6* gene dose had no effect on the accelerated tumor development in the Eμ-myc lymphoma mouse model, despite a noticeable effect of *Traf6* haploinsufficiency on aberrant splenic myeloproliferation, proinflammatory cytokine production, and hepatic immune cell infiltrates in *miR-146a*$^{-/-}$ mice. Thus, it appears that miR-146a engages a different molecular target, and not *Traf6*, to control malignant transformation of B cells. This conclusion is supported by the findings of Contreras et al. (11), who also observed an accelerated B cell lymphomagenesis in the Eμ-myc transgenic mice upon *miR-146a* deletion, but found no major change in NF-κB–dependent signaling in *miR-146a*–deficient tumors. Instead, Contreras et al. proposed that *miR-146a* suppresses tumorigenesis by downregulating expression of EGR1, a transcription factor associated with cellular proliferation and survival. However, *Egr1* is unlikely to function as a direct miR-146a molecular target in mouse cells, because the miR-146a seed sequence in the mouse *Egr1* 3′UTR is not conserved. *Syk*, a critical signaling mediator downstream of B cell antigen receptor, is another potential target through which *miR-146a* may impact B cell proliferation. Abrogation of *miR-146a*–mediated repression of SYK was recently implicated as a major driving factor in *Hoxa9*/*Meis1*-induced mouse model of myeloid leukemogenesis (38). Although this exact target interaction may not be applicable to human leukemias because of the lack of any miR-146a binding sites in the human *Syk* 3′UTR, it is illustrative of the potential role of *miR-146a* dysfunction in driving a variety of human cancers. The list of bioinformatically defined miR-146a targets is relatively rich in genes that are known to contribute to the regulation of cellular growth and, thus, future genetic experiments will be required to identify the key molecular targets through which *miR-146a* exerts its tumor-suppressor activity in different immune cells.

As in the case of tumor suppression, the *miR-146a*–mediated regulation of HSC homeostasis is apparently not dependent on its ability to downmodulate *Traf6* expression. We found no rescue of the progressive BM failure phenotype in *miR-146a*$^{-/-}$ mice with *Traf6* haploinsufficiency. In contrast, our genetic analysis implicated *IFN-γ* as a critical driver of the HSC destruction and resulting pancytopenia in *miR-146a*$^{-/-}$ mice. The strong negative effect of chronic *IFN-γ* production on HSC maintenance is a well-established notion (22, 23, 39). Our data reveal that resident T cells are the most likely source of the aberrant IFN-γ in *miR-146a*$^{-/-}$ BM. This finding is in line with our previous observations that CD4^{+} T cells in *miR-146a*$^{-/-}$ mice are skewed toward Th1 phenotype and secrete excessive amounts of IFN-γ upon activation (13). Furthermore, the role of *miR-146a*–deficient T cells in the progressive BM failure phenotype is supported by the partial rescue of this defect in *miR-146a*$^{-/-}$ mice with a severe depletion of mature lymphocytes because of either *Rag2* or *Rag1* deletion [Fig. 5*F* and data from Zhao et al. (10), respectively].

Presumably, IFN-γ is not the only mediator of inflammation that contributes to the destruction of the HSC niche in *miR-146a*$^{-/-}$ BM. Ablation of *Il-6*, a proinflammatory cytokine also found to be overproduced in *miR-146a*–deficient BM, was shown to rescue the progressive BM failure phenotype in *miR-146a*$^{-/-}$ mice (10). The primary cellular targets and the hierarchical framework between these two cytokines in HSC homeostasis are not yet clear. Interestingly however, IFN-γ–mediated stimulation of the HSC niche in response to an acute viral infection was dependent on IL-6 production by mesenchymal stromal cells in the BM (40). Cytotoxic T cells exposed to a viral antigen apparently secrete IFN-γ to promote IL-6 production by mesenchymal stromal cells that in its turn stimulates multipotent hematopoietic progenitors in the BM and triggers emergency myelopoiesis. Collectively, our observations strongly suggest that the progressive BM failure in *miR-146a*$^{-/-}$ mice is an HSC-extrinsic defect closely resembling the pathophysiological changes during AA. Similar to the situation with *miR-146a*$^{-/-}$ mice, AA is associated with an expansion of autoreactive T cells and, hence, is responsive to immunosuppressive therapies. AA patients exhibit increased levels of circulating IFN-γ, while blockade of this cytokine significantly improves hematopoietic colony-forming activity of the BM cells from afflicted subjects (24). Moreover, a genetic polymorphism that enhances IFN-γ production is strongly associated with the risk of developing AA (41).

Our inference about the nonessential role of *Traf6* as a miR-146a target in the progressive BM failure and lymphoma phenotypes has one potential caveat. It is certainly conceivable that lowering the *Traf6* gene dose did not sufficiently reduce expression of this adapter protein in all relevant *miR-146a*$^{-/-}$ cell types, thus explaining the lack of rescue of some defects in *miR-146a*$^{-/-}$*Traf6*$^{+/-}$ mice. However, in the instance of progressive BM failure, this argument is not very compelling, because our data indicate that HSC destruction in *miR-146a*$^{-/-}$ mice is driven by aberrantly activated T cells; therefore, it is not obvious why *Traf6* haploinsufficiency, while having a profound effect on other T cell-dependent defects in *miR-146a*$^{-/-}$ mice, would have little impact on BM failure. Of note, our conclusion on the role of *Traf6* runs contrary to some observations that implicated this adapter molecule in the regulation of HSC homeostasis and the pathophysiology of MDS (10, 41, 42).

The identity of the molecular target that miR-146a engages in T cells to regulate IFN-γ production is currently unknown. One putative candidate is *Irak1*, because of its ability to trigger activation of the inflammasome and subsequent IL-18 production (43, 44). IL-18 is known to stimulate IFN-γ secretion and *Irak1*-deficient memory CD8^{+} T cells are severely compromised in IFN-γ production. Alternatively, *miR-146a* could target *Stat1* to control IFN-γ expression. As was previously reported, effector CD4^{+} T cells from *miR-146a*$^{-/-}$*Stat1*$^{+/-}$ mice display significantly attenuated levels of IFN-γ production (13).

Collectively, our genetic analysis suggests that separation of function at the level of *miR-146a* can explain its capacity to regulate diverse immunological processes (Fig. 7). This mode of regulation is not unique to *miR-146a* and is apparently used by other immunological miRNAs with pleotropic functions. For example, *miR-155* can interfere with Th2 differentiation by modulating levels of *c-Maf* (45), regulate plasma cell differentiation through PU.1 (46), and control generation and function of

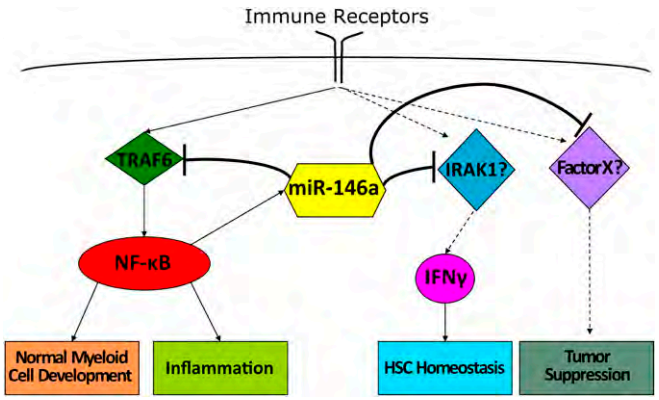

Fig. 7. Separation of function at the level of molecular targets allows *miR-146a* to control multiple immunological functions. Graphical model describing molecular mechanisms by which *miR-146a* regulates inflammation, myeloproliferation, HSC homeostasis, and cancer.

follicular helper T cells by targeting *Peli1* (47). In addition, the *miR-142–BAFF-R* signaling axis was implicated in the control of peripheral B cell proliferation, but was found to be dispensable for the regulation of B cell effector responses (48). As the understanding and awareness of specialized immune cell subsets increases, it is crucial to precisely explicate what mechanisms control and engage their unique gene-expression programs. Opportunities for more precise targeted interventions will arise if there are miRNA-target gene pairings that can be identified as interacting only in a particular cell type or under a certain gene expression program. Once better understood, this cell- and context-specific regulation of cognate targets by miRNAs can be effectively exploited to generate novel therapeutic approaches to treat various immune-related diseases and cancer.

Materials and Methods

Mice. Mice with a homozygous deletion of the *miR-146* gene were generated as previously described (2). Wild-type littermates generated during the initial creation of the *miR-146a* knockout mice were used as wild-type controls (*miR-146a*$^{+/+}$). *miR-146a*$^{-/-}$ mice were mated to mice bearing a heterozygous deletion of *Traf6* (17) to create mice with the *miR-146a*$^{-/-}$*Traf6*$^{+/-}$ genotype. To create the *miR-146a*$^{-/-}$*IFN-γ*$^{-/-}$ double-knockout mouse, *miR-146a*$^{-/-}$ mice were mated to mice with a homozygous deletion of *IFN-γ* (obtained from the Jackson Laboratories) (25).

Male Tg(Eμ-myc) mice (19) were purchased from the Jackson Laboratories and bred to female *miR-146a*$^{-/-}$ mice to produce the Tg(Eμ-myc);*miR-146a*$^{-/-}$ strain. Male Tg(Eμ-myc);*miR-146a*$^{-/-}$ mice were mated with female *miR-146a*$^{-/-}$*Traf6*$^{+/-}$ mice to produce the Tg(Eμ-myc);*miR-146a*$^{-/-}$*Traf6*$^{+/-}$ line.

Mice were housed at the Beckman Research Institute of the City of Hope in accordance with stated Institutional Review Board and Institutional Animal Care and Use Committee (IACUC) protocols (49).

Genomic PCR. DNA was extracted from clipped tails using the KAPA Express Extract buffer (KAPA Biosystems). PCR to detect *Traf6* and *miR-146a* alleles was performed using the KAPA2G Fast Genotyping Mix (KAPA Biosystems) and using primers that were previously reported (2, 17).

Western Blots. Mouse spleens were dissociated through a 45-μm mesh and treated with red blood counts (RBC) lysis buffer (BioLegend). Following RBC lysis and washing, single-cell suspensions of the remaining cells were made in complete RPMI medium containing 10% (vol/vol) FBS along with penicillin and streptomycin. Portions of this single-cell splenocyte suspension were pelleted, washed twice with PBS to remove excess medium, and lysed in cOmplete EDTA-free lysis buffer supplemented with cOmplete EDTA-free protease inhibitor mixture and Phos-Stop phosphatase inhibitor mixture (Roche). Total protein extract concentration was determined using the Bradford dye-binding reagent (Bio-Rad). Samples were run on an SDS-PAGE gel using 20 μg of protein per sample and transferred to nitrocellulose membranes. Anti-TRAF6 antibody (Cat# 597; MBL) was used to detect mouse TRAF6 protein, anti–phospho-IκBα antibody (Cat# 2859; Cell Signaling Technologies) was used to detect phosphorylated IκBα, anti–phospho-p38 MAPK antibody (Cat# 9215; Cell Signaling Technologies) was used to detect phosphorylated p38 MAPK. ImageJ software was used to quantify the relative amounts of TRAF6, phospho-IκBα, and phospho-p38 MAPK normalized to β-actin.

Flow Cytometry. Single-cell suspensions from mouse spleens were prepared as described for BM cells in Western blot sections. One-million cells per sample of a single-cell suspension were stained with appropriate cell-surface markers and analyzed on a BD Accuri C6 flow cytometer. Fluorochrome conjugated antibodies against CD11b, GR1, Ter119, CD4, CD8, CD44, CD6L, CD69, CD150, CD48, CD117, Sca1, CSF1R, F480, were purchased from Biolegend or eBioscience and used according to the manufacturer's instructions.

BMDM Proliferation. BM cells from 10-wk-old female *miR-146*$^{+/+}$, *miR-146a*$^{-/-}$, and *miR-146a*$^{-/-}$*Traf6*$^{+/-}$ mice were plated in triplicate on a 96-well plate at a density of 2×10^4 cells per well. Cells were cultured in complete DMEM supplemented with 50 ng/mL M-CSF. Proliferation of BMDMs was measured using the MTS assay (CellTiter 96; Promega) on day 3 postplating. For quantification of CSF1R, BM cells were plated in six-well dishes at a density of 6×10^5 cells per well. Cells were cultured in complete DMEM supplemented with 50 ng/mL M-CSF with a complete wash and change of medium on day 4.

Sublethal LPS Challenge. Mice were injected intraperitoneally with LPS at a dose of 1 mg/kg of body weight. Peripheral blood was collected by retro-orbital bleeding before LPS injection as well as at 2- and 6-h post-LPS injection. At 24-h postinjection the mice were euthanized and blood was collected via cardiac puncture. Serum separator microtainer tubes (BD) were used to separate serum from whole blood.

Cytokine ELISA. Sandwich ELISAs were performed using 96-well Maxisorp flat bottom plates (NUNC). Cytokine levels in mouse serum were detected using specific anti–IL-6 or anti–TNF-α capture and detection antibodies (eBioscience). Absolute cytokine levels were quantified by comparison with a standard curve produced using either recombinant mouse IL-6 or recombinant mouse TNF-α (eBioscience).

IFN-γ Detection in Stimulated Cells. BM was collected in complete RPMI medium by using a 27-gauge needle to flush out mouse femurs and tibias. Following RBC lysis, the marrow was suspended in complete RPMI medium and plated in a six-well plate at a density of 2×10^6 cells per well. Cells were stimulated with 25 ng of phorbol 12-myristate 13-acetate (Abcam) and 500 ng of Ionomycin (Sigma) for 4 h in the presence of Monensin (BioLegend) to block cytokine secretion. Cells were stained with antibodies against surface markers, then fixed and permeabilized overnight using a fixation and intracellular permeabilization buffer kit (BioLegend). Following permeabilization, cells were stained with anti–IFN-γ antibody and analyzed on an Accuri C6 flow cytometer. Anti-rat IgG1-APC was used as an isotype control.

Histopathology. Freshly harvested tissues were fixed in 10% formalin for 48 h and then washed in 70% ethanol followed by embedding in paraffin blocks, sectioning, and H&E staining. Slides were reviewed by a trained pathologist.

Complete Blood Counts. Whole blood was obtained from freshly euthanized mice via cardiac puncture and analyzed on a Hemavet 950FS (Drew Scientific) within 1 h of collection.

Statistical Analyses. All statistical analysis was performed using Prism 7 (Graphpad Software). *P* values were calculated using a standard ANOVA using Tukey's multiple comparison tests with a single pooled variance. Survival curve comparisons were calculated using the Mantel–Cox log-rank test.

ACKNOWLEDGMENTS. We thank the City of Hope Animal Research Center for their help and care in breeding and maintaining our mouse colonies. Research reported in this publication includes work performed in the Analytical Cytometry Core supported by the National Cancer Institute of the NIH under Award P30CA033572. This work was funded in part by the Nesvig Lymphoma Research Fund at the City of Hope and the Research Career Development award (to M.P.B.) by the STOP CANCER Foundation. The content is solely the responsibility of the authors and does not necessarily represent the official views of the NIH.

1. Boldin MP, Baltimore D (2012) MicroRNAs, new effectors and regulators of NF-κB. *Immunol Rev* 246:205–220.
2. Boldin MP, et al. (2011) miR-146a is a significant brake on autoimmunity, myeloproliferation, and cancer in mice. *J Exp Med* 208:1189–1201.
3. Taganov KD, Boldin MP, Chang KJ, Baltimore D (2006) NF-kappaB-dependent induction of microRNA miR-146, an inhibitor targeted to signaling proteins of innate immune responses. *Proc Natl Acad Sci USA* 103:12481–12486.
4. Zhao JL, et al. (2011) NF-kappaB dysregulation in microRNA-146a-deficient mice drives the development of myeloid malignancies. *Proc Natl Acad Sci USA* 108: 9184–9189.
5. Nakasa T, et al. (2008) Expression of microRNA-146 in rheumatoid arthritis synovial tissue. *Arthritis Rheum* 58:1284–1292.
6. Tang Y, et al. (2009) MicroRNA-146A contributes to abnormal activation of the type I interferon pathway in human lupus by targeting the key signaling proteins. *Arthritis Rheum* 60:1065–1075.
7. Pauley KM, et al. (2011) Altered miR-146a expression in Sjögren's syndrome and its functional role in innate immunity. *Eur J Immunol* 41:2029–2039.
8. Zhao JL, Starczynowski DT (2014) Role of microRNA-146a in normal and malignant hematopoietic stem cell function. *Front Genet* 5:219.
9. Starczynowski DT, et al. (2010) Identification of miR-145 and miR-146a as mediators of the 5q- syndrome phenotype. *Nat Med* 16:49–58.
10. Zhao JL, Rao DS, O'Connell RM, Garcia-Flores Y, Baltimore D (2013) MicroRNA-146a acts as a guardian of the quality and longevity of hematopoietic stem cells in mice. *eLife* 2:e00537.
11. Contreras JR, et al. (2015) MicroRNA-146a modulates B-cell oncogenesis by regulating Egr1. *Oncotarget* 6:11023–11037.
12. Labbaye C, Testa U (2012) The emerging role of MIR-146A in the control of hematopoiesis, immune function and cancer. *J Hematol Oncol* 5:13.
13. Lu LF, et al. (2010) Function of miR-146a in controlling Treg cell-mediated regulation of Th1 responses. *Cell* 142:914–929.
14. Labbaye C, et al. (2008) A three-step pathway comprising PLZF/miR-146a/CXCR4 controls megakaryopoiesis. *Nat Cell Biol* 10:788–801.
15. Crone SG, et al. (2012) MicroRNA-146a inhibits G protein-coupled receptor-mediated activation of NF-κB by targeting CARD10 and COPS8 in gastric cancer. *Mol Cancer* 11:71.
16. Yang L, et al. (2012) miR-146a controls the resolution of T cell responses in mice. *J Exp Med* 209:1655–1670.
17. Naito A, et al. (1999) Severe osteopetrosis, defective interleukin-1 signalling and lymph node organogenesis in TRAF6-deficient mice. *Genes Cells* 4:353–362.
18. Kobayashi N, et al. (2001) Segregation of TRAF6-mediated signaling pathways clarifies its role in osteoclastogenesis. *EMBO J* 20:1271–1280.
19. Harris AW, et al. (1988) The E mu-myc transgenic mouse. A model for high-incidence spontaneous lymphoma and leukemia of early B cells. *J Exp Med* 167:353–371.
20. Eischen CM, Weber JD, Roussel MF, Sherr CJ, Cleveland JL (1999) Disruption of the ARF-Mdm2-p53 tumor suppressor pathway in Myc-induced lymphomagenesis. *Genes Dev* 13:2658–2669.
21. Langdon WY, Harris AW, Cory S, Adams JM (1986) The c-myc oncogene perturbs B lymphocyte development in E-mu-myc transgenic mice. *Cell* 47:11–18.
22. de Bruin AM, Voermans C, Nolte MA (2014) Impact of interferon-γ on hematopoiesis. *Blood* 124:2479–2486.
23. Baldridge MT, King KY, Boles NC, Weksberg DC, Goodell MA (2010) Quiescent haematopoietic stem cells are activated by IFN-gamma in response to chronic infection. *Nature* 465:793–797.
24. Zoumbos NC, Gascon P, Djeu JY, Young NS (1985) Interferon is a mediator of hematopoietic suppression in aplastic anemia in vitro and possibly in vivo. *Proc Natl Acad Sci USA* 82:188–192.
25. Dalton DK, et al. (1993) Multiple defects of immune cell function in mice with disrupted interferon-gamma genes. *Science* 259:1739–1742.
26. Zhao E, et al. (2012) Bone marrow and the control of immunity. *Cell Mol Immunol* 9: 11–19.
27. Walsh MC, Lee J, Choi Y (2015) Tumor necrosis factor receptor- associated factor 6 (TRAF6) regulation of development, function, and homeostasis of the immune system. *Immunol Rev* 266:72–92.
28. Cao Z, Xiong J, Takeuchi M, Kurama T, Goeddel DV (1996) TRAF6 is a signal transducer for interleukin-1. *Nature* 383:443–446.
29. Ishida T, et al. (1996) Identification of TRAF6, a novel tumor necrosis factor receptor-associated factor protein that mediates signaling from an amino-terminal domain of the CD40 cytoplasmic region. *J Biol Chem* 271:28745–28748.
30. Ward C, et al. (1999) NF-kappaB activation is a critical regulator of human granulocyte apoptosis in vitro. *J Biol Chem* 274:4309–4318.
31. Huxford T, Malek S, Ghosh G (1999) Structure and mechanism in NF-kappa B/I kappa B signaling. *Cold Spring Harb Symp Quant Biol* 64:533–540.
32. May MJ, Ghosh S (1999) IkappaB kinases: Kinsmen with different crafts. *Science* 284: 271–273.
33. Shepard LW, et al. (2001) Constitutive activation of NF-kappa B and secretion of interleukin-8 induced by the G protein-coupled receptor of Kaposi's sarcoma-associated herpesvirus involve G alpha(13) and RhoA. *J Biol Chem* 276:45979–45987.
34. Bosman MC, Schuringa JJ, Vellenga E (2016) Constitutive NF-κB activation in AML: Causes and treatment strategies. *Crit Rev Oncol Hematol* 98:35–44.
35. Pham LV, Tamayo AT, Yoshimura LC, Lin-Lee YC, Ford RJ (2005) Constitutive NF-kappaB and NFAT activation in aggressive B-cell lymphomas synergistically activates the CD154 gene and maintains lymphoma cell survival. *Blood* 106:3940–3947.
36. Karin M, Cao Y, Greten FR, Li ZW (2002) NF-kappaB in cancer: From innocent bystander to major culprit. *Nat Rev Cancer* 2:301–310.
37. Kim DW, et al. (2000) Activation of NF-kappaB/Rel occurs early during neoplastic transformation of mammary cells. *Carcinogenesis* 21:871–879.
38. Mohr S, et al. (2017) Hoxa9 and Meis1 cooperatively induce addiction to Syk signaling by suppressing miR-146a in acute myeloid leukemia. *Cancer cell* 31:549–562 e511.
39. Chen J, Feng X, Desierto MJ, Keyvanfar K, Young NS (2015) IFN-γ-mediated hematopoietic cell destruction in murine models of immune-mediated bone marrow failure. *Blood* 126:2621–2631.
40. Schürch CM, Riether C, Ochsenbein AF (2014) Cytotoxic CD8+ T cells stimulate hematopoietic progenitors by promoting cytokine release from bone marrow mesenchymal stromal cells. *Cell Stem Cell* 14:460–472.
41. Dufour C, et al.; Associazione Italiana di Emato-Oncologia Pediatrica (AIEOP); Department of Hematology, Ospedale S. Martino, Genoa, Italy (2004) Homozygosis for (12) CA repeats in the first intron of the human IFN-gamma gene is significantly associated with the risk of aplastic anaemia in Caucasian population. *Br J Haematol* 126: 682–685.
42. Varney ME, et al. (2015) Loss of Tifab, a del(5q) MDS gene, alters hematopoiesis through derepression of Toll-like receptor-TRAF6 signaling. *J Exp Med* 212: 1967–1985.
43. Fernandes-Alnemri T, et al. (2013) Cutting edge: TLR signaling licenses IRAK1 for rapid activation of the NLRP3 inflammasome. *J Immunol* 191:3995–3999.
44. Lin KM, et al. (2014) IRAK-1 bypasses priming and directly links TLRs to rapid NLRP3 inflammasome activation. *Proc Natl Acad Sci USA* 111:775–780.
45. Su W, et al. (2014) The p53 transcription factor modulates microglia behavior through microRNA-dependent regulation of c-Maf. *J Immunol* 192:358–366.
46. Lu D, et al. (2014) The miR-155-PU.1 axis acts on Pax5 to enable efficient terminal B cell differentiation. *J Exp Med* 211:2183–2198.
47. Liu WH, et al. (2016) A miR-155-Peli1-c-Rel pathway controls the generation and function of T follicular helper cells. *J Exp Med* 213:1901–1919.
48. Kramer NJ, et al. (2015) Altered lymphopoiesis and immunodeficiency in miR-142 null mice. *Blood* 125:3720–3730.
49. National Research Council (2011) *Guide for the Care and Use of Laboratory Animals* (National Academies Press, Washington, DC), 8th Ed.